Published online 20 July 2009

Nucleic Acids Research, 2009, Vol. 37, No. 17 ***5589–5601***
doi:10.1093/nar/gkp598

Conformationally rigid nucleoside probes help understand the role of sugar pucker and nucleobase orientation in the thrombin-binding aptamer

Hisao Saneyoshi[1], Stefania Mazzini[2], Anna Aviñó[3], Guillem Portella[4], Carlos González[5], Modesto Orozco[4], Víctor E. Marquez[1,*] and Ramon Eritja[3,*]

[1]Laboratory of Medicinal Chemistry, Center for Cancer Research, National Cancer Institute at Frederick, Frederick, MD 21702, USA, [2]DISMA, Universita' degli Studi di Milano. Via Celoria 2, I-20133 Milano, Italy, [3]Institute for Research in Biomedicine, IQAC-CSIC, CIBER-BBN Networking Centre on Bioengineering, Biomaterials and Nanomedicine, Baldiri Reixac 15, E-08028 Barcelona, [4]Joint IRB-BSC program on Computational Biology. Institute for Research in Biomedicine, Baldiri Reixac 10-12, E-08028 Barcelona and Barcelona Supercomputing Center, Jordi Girona 29, 08034 Barcelona, Department of Biochemistry, University of Barcelona, Diagonal 647, 08028 Barcelona, [5]Instituto de Química Física Rocasolano. CSIC, C/Serrano, 119, 28006 Madrid, Spain

Received April 23, 2009; Revised June 29, 2009; Accepted June 30, 2009

ABSTRACT

Modified thrombin-binding aptamers carrying 2′-deoxyguanine (dG) residues with locked *North*- or *South*-bicyclo[3.1.0]hexane pseudosugars were synthesized. Individual 2′-deoxyguanosines at positions dG5, dG10, dG14 and dG15 of the aptamer were replaced by these analogues where the *North*/*anti* and *South*/*syn* conformational states were confined. It was found that the global structure of the DNA aptamer was, for the most part, very accommodating. The substitution at positions 5, 10 and 14 with a locked *South*/*syn*-dG nucleoside produced aptamers with the same stability and global structure as the innate, unmodified one. Replacing position 15 with the same *South*/*syn*-dG nucleoside induced a strong destabilization of the aptamer, while the antipodal *North*/*anti*-dG nucleoside was less destabilizing. Remarkably, the insertion of a *North*/*anti*-dG nucleoside at position 14, where both pseudosugar conformation and glycosyl torsion angle are opposite with respect to the native structure, led to the complete disruption of the G-tetraplex structure as detected by NMR and confirmed by extensive molecular dynamics simulations. We conclude that conformationally locked bicyclo[3.1.0]hexane nucleosides appear to be excellent tools for studying the role of key conformational parameters that are critical for the formation of a stable, antiparallel G-tetrad DNA structures.

INTRODUCTION

Aptamers are oligonucleotides that were originally derived from an *in vitro* evolution process known as SELEX (systematic evolution of ligands by exponential enrichment) (1,2), which selects them on the basis of their specific and tight binding affinity to a ligand of choice from a library of sequences. Through this approach, large number of aptamers with very high affinity have been developed for diagnostic, therapeutic and other technical applications (3), but there is still room for improvement in terms of increasing their binding properties and stability to nucleases (4). One of the most studied aptamers is the 15-base long thrombin-binding aptamer (TBA), 5′-$G^1G^2T^3T^4G^5G^6T^7G^8T^9G^{10}G^{11}T^{12}T^{13}G^{14}G^{15}$-3′ (5). This oligonucleotide binds specifically to thrombin at nanomolar concentrations, and for this reason it has interesting anticoagulant properties (5,6). TBA is characterized (both in the thrombin bound and unbound forms) by a chair-like, antiparallel quadruplex structure consisting of two G-tetrads connected by two TT loops and a single TGT loop (7–11) (Figure 1). The antiparallel quadruplex structure of TBA has a distinctive denaturation–renaturation profile that is reversible and observable by different techniques, particularly by NMR experiments, which suggests that the denaturation of the quadruplex occurs by opening of the G–G base pairs that are not protected by a loop, followed by the opening the

*To whom correspondence should be addressed. Tel: +34 93 4039942; Fax: +34 93 2045904; Email: recgma@cid.csic.es
Correspondence may also be addressed to Víctor E. Marquez. Tel: +1 301 8465954; Fax: +1 301 8466033; Email: marquezv@mail.nih.giv

The authors wish it to be known that, in their opinion, the first four authors should be regarded as joint first authors.

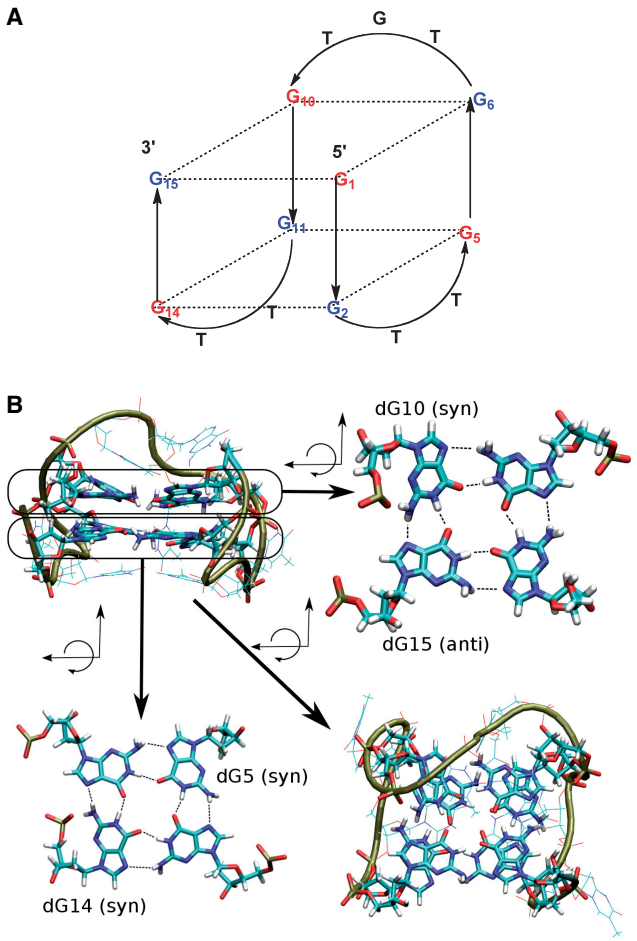

Figure 1. (**A**) Schematic representation of the antiparallel folding of the thrombin-binding aptamer (TBA); blue represents guanines that are *anti* and red guanines that are *syn*. Positions of 5, 10, 14 and 15 were modified in this study. (**B**) Molecular representation: the upper left quadrant shows a lateral view of the TBA and the lower right quadrant a view from the top of the molecule [dG5(syn) and dG14(anti) in the lower quartet as well as dG10(syn) and dG15(syn) in the upper quartet are indicated].

TGT loop (12). The conformational distribution of 2′-deoxyguanosines in the G-quartets of the TBA aptamer is well defined. All sugar puckers are *South (S)*, while the guanines on the same G-quartet plane display alternating *syn*/*anti* conformations with respect to the glycosyl torsion angle (*syn*-dG at positions dG1, dG5, dG10 and dG14; *anti*-dG at positions dG2, dG6, dG11 and dG15, Figure 1). It is worth noting that despite the robust stability of the intramolecular quadruplex structure, alternative intermolecular tetraplexes are possible at high aptamer concentration, as detected by CD and electrophoresis migration experiments (13).

Historically, several modified TBAs have been synthesized containing different types of nucleobase modifications introduced by 2′-deoxyinosine (8), 2′-deoxy-6-thioguanosine (14) and 8-amino-2′-deoxyguanosine (15) residues. Other modifications included the insertion of 5′–5′ inversion sites (16,17), the incorporation of locked nucleic acids, LNA (18,19), 2′-deoxy-2′-fluoro-D-arabino-nucleic acids, 2′-F-ANA (20) and ribonucleotides (21).

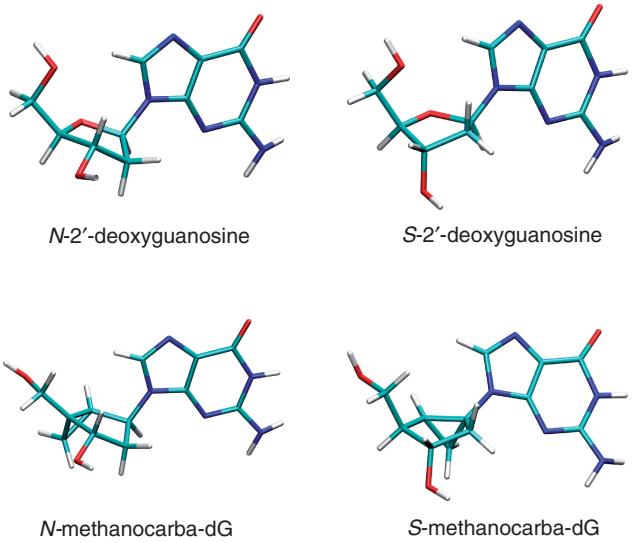

Figure 2. Effect of the fused cyclopropane ring in locking the *N*- and *S*-conformations of the embedded cyclopentane ring of methanocarba-dG nucleosides closely mimicking the conformations of natural *N*- and *S*-2′-deoxyguanosines. For the sake of clarity only *anti* conformers are shown.

Many of these modified nucleotides allowed a certain control of the sugar ring pucker, favouring either an RNA-like C3′-*endo* (*North*, *N*) conformation or a DNA-like C2′-*endo* (*South*, *S*) conformation. Use of modified LNAs (22–26) has helped to achieve complete conformational control due to the presence of a methylene bridge between the 2′-oxygen and the 4′-carbon (27). This bridge creates a rigid bicyclic structure where the embedded furanose ring is 'locked' in the *N* conformation. Prior to LNAs, the first synthesis of a conformationally locked nucleoside analogue was based on a carbocyclic bicyclo[3.1.0]hexane template (28). This template was later used in the construction of a single DNA strand carrying several *N*-locked methanocarba thymidine units which hybridized efficiently with its complementary RNA strand (29) and the synthesis of other oligonucleotides carrying *N*- and *S*-locked versions of 2′-deoxymethanocarba adenosine, methanocarba thymidine and abasic sites (30,31). An advantage of this methanocarba nucleoside system over LNAs is that both *N*- and *S*-locked platforms can be prepared by shifting the position of the fused cyclopropane ring (29) (Figure 2). Later, additional data suggested that the addition of *N*-locked methanocarba nucleosides to a standard B-DNA duplex could cause bending towards the minor groove (32,33), while incorporation of *S*-locked methanocarba nucleosides into a similar standard DNA produced a more complicated equilibrium between different duplex forms, where the major component was a duplex with a slightly higher thermodynamic stability than the unmodified duplex (34).

In this article, we describe the effects of replacing a single 2′-deoxyguanosine residue of the TBA (positions dG5, dG10, dG14 and dG15; see Figure 1) with methanocarba nucleosides locked in either the *N*- or *S*-conformation. These positions were selected to explore

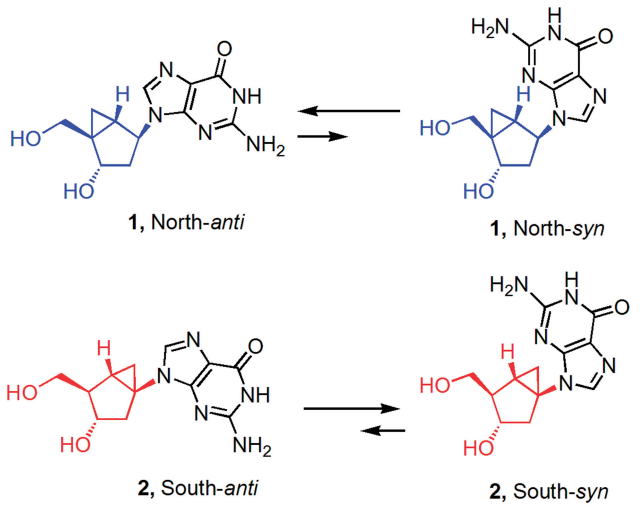

Figure 3. Biased *anti-syn* equilibrium of conformationally restricted *North* (blue) and *South* (red) methanocarba-dG nucleosides.

the combined effects of a constrained sugar pucker (*N* or *S*) and the corresponding biased glycosyl torsion angle (*anti* or *syn*) associated with a particular pseudosugar conformation. In conventional nucleosides, the glycosyl torsion angle is weakly associated with a specific sugar pucker: the *syn* conformation is associated with a *S*-sugar pucker, while for the *anti* conformation both *N*- and *S*-sugar puckers are equally probable (35). For methanocarba nucleosides, these associated preferences are enhanced due to the steric consequences introduced by the rigid pseudosugar ring and its effect on the rotation of the glycosyl bond. Indeed, both experimental and theoretical results [see (36) and results below] indicate that a *N*-pseudosugar conformation favours the *anti* glycosyl orientation, whereas the *S*-pseudosugar conformation favours the *syn* disposition of the base. Therefore, we anticipated that the introduction of methanocarba nucleosides with locked-*N*(*anti*) and locked-*S*(*syn*) conformations could fix the conformational state of these nucleosides and help us understand the impact of conformational restrictions on the antiparallel, G-quartet DNA structure of TBA (Figure 3).

We thus prepared six modified TBA derivatives: (i) TBA-dG5*S*, (ii) TBA-dG10*S*, (iii) TBA-dG14*S* carrying the *S*-pseudosugar (same sugar puckering and *syn* glycosyl bond orientation as in unmodified TBA); (iv) TBA-dG15*S* carrying the same *S*-pseudosugar at position 15 (same sugar puckering as in native TBA, but opposite *syn* glycosyl conformation); (v) TBA-dG14*N* carrying the *N*-pseudosugar at position 14 (opposite sugar puckering and opposite glycosyl conformation relative to native TBA) and (vi) TBA-dG15*N* carrying the *N*-pseudosugar at position 15 (opposite sugar puckering but similar *anti* glycosyl conformation as in normal TBA) (5). The substitution at position 14 of the aptamer with a locked *S*-dG produced a modified aptamer with the same stability and global structure as the unmodified aptamer as confirmed by NMR and molecular dynamics simulations. Replacing position 15 for a similarly locked *S*-dG induced a strong destabilization of the aptamer, while the antipodal *N*-dG produced a somewhat lower destabilization; however, in both cases the global structure was reasonably preserved. In sharp contrast, the substitution at position 14 with *N*-dG produced a dramatic disruption in the aptamer structure, which was clearly observable by NMR and state-of-the-art molecular dynamics simulations. This last observation clearly shows that the combination of the wrong sugar pucker and the wrong *anti* conformation at this position is largely destabilizing to the entire tetraplex architecture.

The structural properties of these locked pseudosugars are therefore useful for exploring the role of the sugar pucker and the glycosyl bond orientation in the stabilization of G-quartet DNA structures.

MATERIALS AND METHODS

General methods of chemical synthesis

The general methods of synthesis and the specific preparation and characterization of all the compounds in Schemes 1 and 2 are included in the Supplementary Data.

Oligonucleotide synthesis and purification

The syntheses of the oligonucleotides TBA: d(5′-GGT TGG TGT GGT TGG-3′); TBA-dG15*N*: d(5′-GGT TGG TGT GGT TG<u>G</u>-3′), <u>G</u>: *N*-dG; TBA-dG15*S*: d(5′-GGT TGG TGT <u>G</u>GT T<u>G</u>G-3′), <u>G</u>: *S*-dG, TBA-dG14*S*: d(5′-GGT TGG TGT G<u>G</u>T T<u>G</u>G-3′), <u>G</u>: *S*-dG, TBA-dG14*N*: d(5′-GGT TGG TGT G<u>G</u>T T<u>G</u>G-3′), <u>G</u>: *N*-dG, dG5*S*: d(5′-GGT T<u>G</u>G TGT GGT T<u>G</u>G-3′), <u>G</u>: *S*-dG and dG10*S*: d(5′-GG<u>T</u> TGG TGT <u>G</u>GT TGG-3′), <u>G</u>: *S*-dG are described in the Supplementary Data.

NMR spectroscopy

The samples of TBA derivatives for NMR measurements were dissolved in 500 µl H_2O/D_2O (9:1) or D_2O containing 10 mM potassium phosphate buffer and 5 mM KCl (pH 6.9), corresponding to a G-quadruplex concentration of 0.8 mM. NMR spectra were performed at temperatures ranging between 5°C and 65°C on a Bruker AV-600 spectrometer, equipped with a *z*-gradient triple resonance cryoprobe and processed with TOPSPIN v. 1.3. Chemical shifts (δ) were measured in ppm. ^{1}H NMR spectra were referenced to external DSS (2,2-dimethyl-2--silapentane-5-sulfonate sodium salt) set at 0.00 ppm. 1D and 2D spectra were recorded, in the case of D_2O solutions, with water suppression obtained by presaturation pulse sequences, while, in the case of H_2O/D_2O (9:1) solutions, using a gradient-based solvent suppression. Two-dimensional homonuclear correlation spectra NOESY (37), and TOCSY (38,39) were acquired using standard pulse sequences in the phase-sensitive mode at 5°C (mixing times and spin lock values of 150 ms and 60 ms, respectively). The program Sparky (40) was used to assign the NOESY cross-peaks.

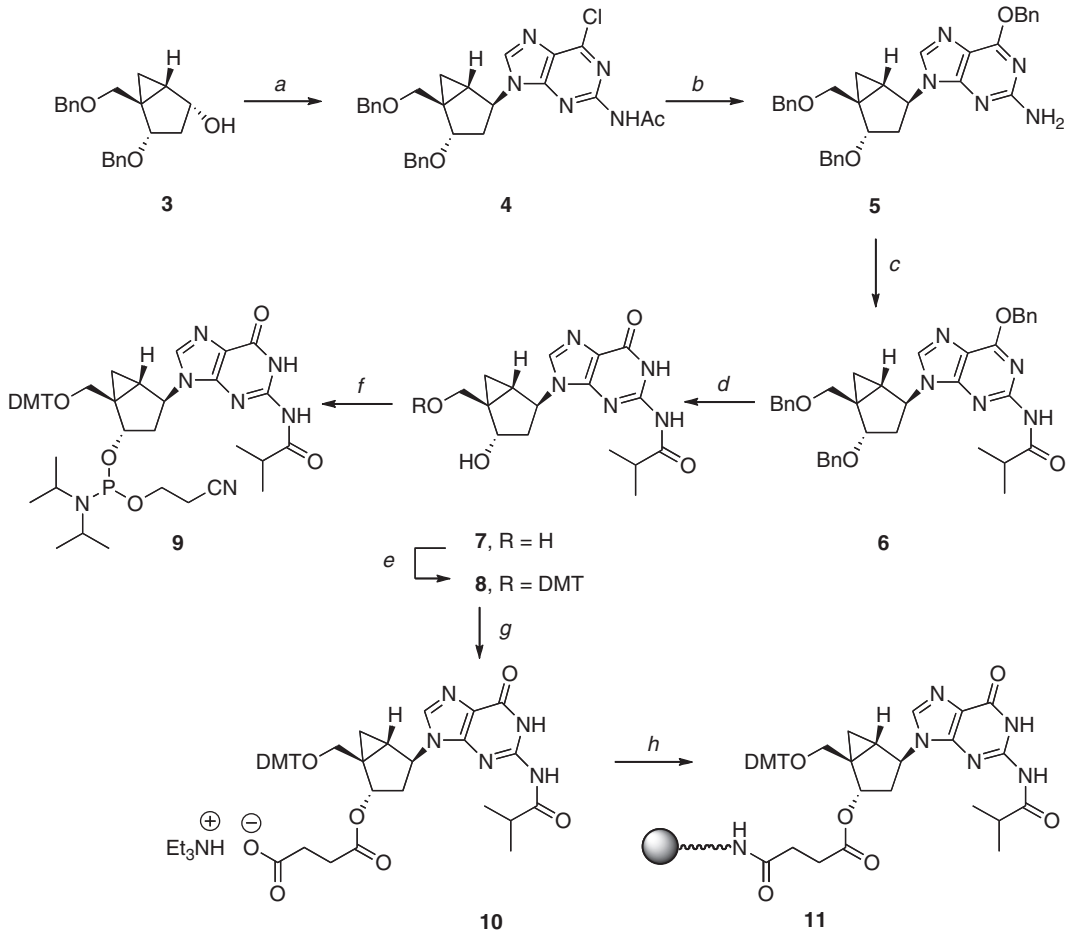

Scheme 1. Reagents and conditions: (**a**) PPh_3, DIAD, 2-acetamide-6-chrolopurine, THF, 0°C, 73%; (**b**) BnONa, BnOH, rt, 89%; (**c**) isobutyryl chloride, pyridine, rt, 84%; (**d**) BCl_3, CH_2Cl_2, –78°C, 69%; (**e**) DMTr-Cl, pyridine, rt, 83%; (**f**) Diisopropylethylamine, 2-cyanoethyl diisopropyl-chlorophosphoramidite, CH_2Cl_2 (**g**) Succinic anhydride, Et_3N, DMAP, CH_2Cl_2, rt, 81%; (**h**) i. LCAA-CPG, DCC, CH_2Cl_2; ii. pyridine:Ac_2O (9:1, v/v), DMAP.

Thermal denaturation experiments of aptamers using UV spectroscopy

The thermal melting curves were performed following the absorption change at 295 nm from 20°C to 80°C with a linear temperature ramp of 0.5°C/min on a JASCO V-650 spectrophotometer equipped with a Peltier temperature control. All measurements were done in triplicate in 10 mM sodium cacodylate buffer and 100 mM KCl (pH 6.9). The concentration of the samples was 6 μM.

Thermal denaturation experiments of aptamers using circular dichroism (CD)

CD spectra were obtained following the change of ellipticity from 220 nm to 320 nm at different temperatures on a Jasco spectropolarimeter equipped with a Peltier temperature control used to set the temperature between 5°C and 75°C. The changes in ellipticity versus temperatures at λ_{max} were plotted and used to obtain the melting temperature. All measurements were conducted in 10 mM potassium phosphate buffer and 5 mM KCl (pH 6.9). The concentration of the samples was 80 μM.

Computational methods

Conformational study of methanocarba 2′-deoxyguanosine derivatives. It is expected that the fusion of the cyclopropane ring through 4′ (using ribose numbering) leads to *N*-type conformers, while its fusion through 1′ leads to the antipodal *S*-type conformers. However, analysis of the structures show that such preferences could change due to the 'boat' $\rightleftarrows$ 'chair' equilibrium of the six member ring (Figure 4). Although electron diffraction microwave spectroscopy (41), X-ray crystallography (22,42,43), as well *ab initio* calculations (44–47) have demonstrated that the boat form is the preferred conformation in a free-standing bicyclo[3.1.0]hexane system, no definitive evidence on the thermodynamics of the 'boat' $\rightleftarrows$ 'chair' equilibrium of G-nucleosides in solution and in nucleic acid environment exists. To clarify this crucial point, we created models of 2′-deoxyguanosine, *N*-methanocarba-dG and *S*-methanocarba-dG in the *syn* and *anti* conformations and evaluated their relative energy with high-level quantum mechanical calculations. For 2′-deoxyguanosine, both *N* and *S* puckerings were considered, while for *N*- and *S*-methanocarba-dG both 'boat'

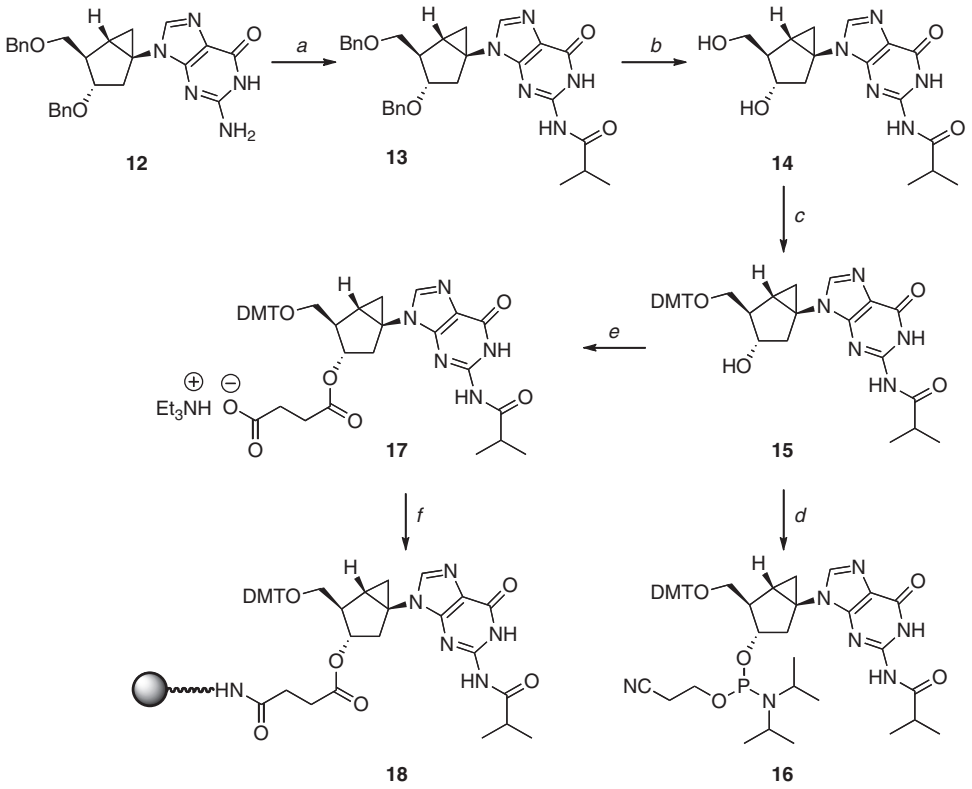

Scheme 2. Reagents and conditions: (**a**) TMS-Cl, isobutyryl chloride, pyridine, rt, 84%; (**b**) H_2, 10% Pd-C, MeOH, rt, 95%; (**c**) DMTr-Cl, Et_3N, pyridine, rt, 83%; (**d**) Diisopropylethylamine, 2-cyanoethyl diisopropylchlorophosphoramidite, CH_2Cl_2; (**e**) Succinic anhydride, Et_3N, DMAP, CH_2Cl_2, rt, 81%; (**f**) (1) LCAA-CPG, EDCl, Et_3N, DMAP, pyridine (2) pyridine:Ac_2O (9:1, V/V), DMAP.

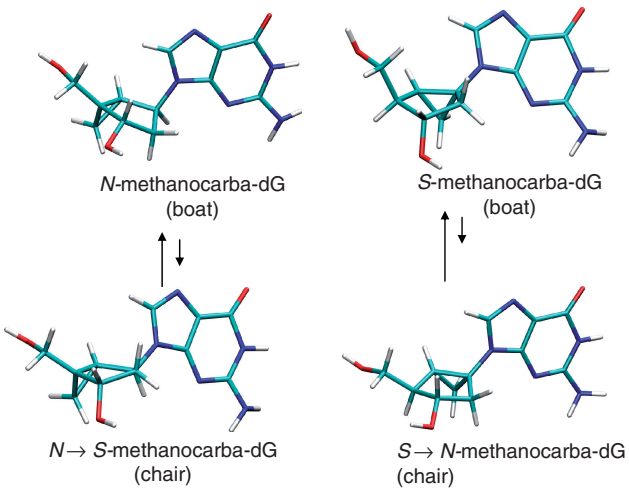

Figure 4. Change in sugar puckering in the embedded cyclopentane ring when the bicyclo[3.1.0]hexane system is allowed to change from its stable 'boat' conformation to the unstable 'chair' conformation.

and 'chair' conformers were studied. In the case of the 'chair' conformers, it is important to recognize that in shifting from 'boat' to 'chair', the puckering of the embedded cyclopentane ring inverts the pseudosugar pucker from *N* to *S* or vice versa (Figure 4). The rest of the internal parameters for the starting geometries (including the C4–C5′ rotation) were taken from those found in a typical G-quartet DNA structure and the starting models were optimized at the B3LYP/6-31G(d) level of theory (48). No restrictions were introduced in the calculations, except for *N*-methanocarba-dG, where the 'chair' conformation needed to be reinforced to avoid spontaneous conformational transitions. Solvent effects were introduced using B3LYP/MST calculations (49–54).

Parametrization of the methanocarba-2′-deoxyguanine derivatives for classical simulations. Classical calculations on the methanocarba-dG derivatives required suitable force-field parameters. Van der Waals, stretching and bending parameters were taken by homology with AMBER force field for nucleic acids (55). Atomic charges were derived from standard RESP/6-31G(d) methodology (56). Torsions not available in the latest version of the AMBER force field were derived by fitting to quantum chemical calculations at the B3LYP/6-31G(d) level. For this purpose, different ring conformations and glycosyl torsion angles were generated using appropriate dihedral restrictions. The corresponding energy differences were fitted by adding suitable torsional parameters to the standard AMBER force field (see below) using an 'in house' Monte Carlo fitting procedure (57). Parmbsc0-adapted (57) parameters for the methanocarba-guanine derivatives are available upon request.

Molecular dynamics (MD) simulations. MD simulations were used to evaluate the structural impact of the presence

of methanocarba-dG (*N* and *S*) derivatives at the different positions in the aptamer, namely: TBA-dG14*N*, TBA-dG15*N*, TBA-dG14*S* and TBA-dG15*S*. We modelled five aptamers, one containing only the natural nucleotides and the remaining containing the different methanocarba-dG derivatives using as template the TBA structure derived by NMR (PDB code 148D (9). Starting geometries were neutralized by adding enough sodium ions (including those needed in the central G-channel) solvated with ~3500 water molecules, optimized, thermalized and equilibrated using our standard multi-stage protocol (57) of doubling the length of individual steps to guarantee stability. Final structures were equilibrated for one additional nanosecond. A short 500 ps run was then used to derive 10 configurations (of the five structures) from which we generated (after velocity randomization and re-equilibration) 10 independent production trajectories that were extended for 10 ns. In cases where all trajectories sampled the same region of the conformational space, they were combined to generate a meta-trajectory. In cases where large conformational transitions happened in same cases, individual trajectories were treated independently.

Interactions between atoms were described by the parmbsc0 refinement of the parm99 force field (55) and TIP3P model (58). The new required parameters were derived as mentioned above. All simulations were carried out using the Gromacs-4 software (59), with periodic boundary conditions and the particle mesh Ewald method (60) for long-range electrostatic treatment and a cut-off radius of 14 Å for short-range repulsive and attractive dispersion interactions, modelled via a Lennard-Jones potential. The Settle algorithm (61) was used to constrain bond lengths and angles of water molecules, and P-LINCS (62) was used for all other bond lengths, allowing an integration time step of 2 fs. The temperature of the simulation was kept constant at 300 K using the uncoupled thermostat strategy of Bussi *et al.* (63). The pressure of the systems was kept constant by weak isotropic coupling to a pressure bath of 1 atm (64). All simulations were carried out at the BSC-MareNostrum supercomputer.

RESULTS AND DISCUSSION

Conformational analysis

Conformational analysis of methanocarba-dG (*N* and *S*) derivatives at the *ab initio* level showed, as expected, that the structures displayed a clear 'boat' preference over the 'chair' conformation (Table 1) and, accordingly, the 'puckering' conformation appears strictly dictated by the placement of the cyclopropane ring in the bicyclo[3.1.0] hexane scaffold as experimentally suggested for related compounds (36,42). The only case where the boat $\rightleftarrows$ chair equilibrium might have some impact is when the *S*-pseudosugar is forced to the *anti* conformation (Table 1), since then the boat/chair difference is not too large (3.1 versus 4.2 kcal/mol in aqueous solution). As experimentally suggested (36,42), in both the solid state and in solution the *N*-pseudosugar favours the *anti* conformation, while the *S*-pseudosugar is biased towards the *syn* conformation. In both cases, the difference found was quite significant (3–4 kcal/mol) indicating that the population of the minor conformer in solution would be negligible (Table 1). Thus, the *S*-pseudosugar template provides a conformation that is closer to that of 2′-deoxyguanosine at position 14 of the TBA. Since it is clear that *S*-pseudosugar is more rigid than the 2′-deoxyribose ring, $S \rightarrow N$ or $syn \rightarrow anti$ transitions are more difficult (Table 1), and hence, both pseudosugar and glycosyl conformations are considered virtually locked (Table 1).

Table 1. Calculated relative energies of different conformers of *N*- and *S*-2′-deoxyguanosine and methanocarba-dG derivatives in the gas phase and in aqueous solution (see 'Materials and Methods' section)

Sugar conformer	Glycosyl torsion	ΔE (vac) (kcal/mol)	ΔE (water) (kcal/mol)
methanocarba-dG-boat (*N*)	*syn*	0.2	3.7
methanocarba-dG-boat (*N*)	*anti*	0.0	0.0
*methanocarba-dG-chair ($N \rightarrow S$)	*syn*	5.3	7.1
*methanocarba-dG-chair ($N \rightarrow S$)	*anti*	4.4	4.7
methanocarba-dG-boat (*S*)	*syn*	0.0	0.0
methanocarba-dG-boat (*S*)	*anti*	8.6	3.1
*methanocarba-dG-chair ($S \rightarrow N$)	*syn*	6.6	4.8
*methanocarba-dG-chair ($S \rightarrow N$)	*anti*	12.5	4.2
2′-deoxyguanosine *N*	*syn*	2.4	2.7
2′-deoxyguanosine *N*	*anti*	7.2	3.3
2′-deoxyguanosine *S*	*syn*	0.0	0.0
2′-deoxyguanosine *S*	*anti*	6.4	2.2

The conformation around the 'C4′–C5′ bond' found during optimization is shown (using by homology the ribose nomenclature). All values are referred to the most stable conformer found in our analysis, and they cannot be compared between different molecules. Star-labelled methanocarba-dG 'chair' derivatives were minimized under dihedral constraints to preserve the chair conformation. In these compounds the change from 'boat' to 'chair' inverts the pseudorotational position of the embedded cyclopentane from *N* to *S* and vice versa.

A word of caution is necessary when extrapolating the conformational preferences of isolated nucleosides to those inside the TBA. However, our theoretical results, as well as experimental data (36,42), strongly suggest that the preferred pseudosugar puckerings will be in the *N* region for *N*-methanocarba-2′-dG and in the *S* hemisphere for the *S*-methanocarba-2′-dG. The *N* compound is likely to be quite unstable in the *syn* region and will be found mostly in the *anti* conformation; the reverse is true for the *S*-compound. Incorporation of the modified methanocarba derivatives at positions of the G-DNA that do not match the conformation of the native structure are thus expected to have a negative impact on stability (and perhaps on the global structure) of the TBA (*vide infra*).

Synthesis of pseudonucleoside derivatives required for oligonucleotide synthesis

The syntheses of plain methanocarba nucleosides *N*-dG (**1**) and *S*-dG (**2**) have been reported (43,65). The required steps to prepare the corresponding *N*-dG phosphoramidite **9** and the CPG-loaded, *N*-dG solid support (**11**) are shown in Scheme 1. Under Mitsunobu conditions, the known precursor **3** (43) reacted with 2-acetamido-6--chloropurine to give the desired coupled product **4** in 73%. Displacement of the 6-chloro group with sodium

benzylate provided compound **5**; this reaction occurred with the simultaneous removal of the *N*-acetyl group. Protection of the free 2-amino group as the *N*-isobutyryl amide **6** was followed by the removal of all benzyl groups with BCl_3 to give compound **7**. From this point onward, conventional 5′-OH protection as the DMT ether **8** and phosphitylation with 2-cyanoethyl diisopropylchlorophosphoramidite provided the desired phosphoramidite building block **9**. From compound **8**, coupling with succinic anhydride gave the 3′-*O*-succinyl derivative **10** which was then loaded onto the CPG resin to give **11**.

For the synthesis of the antipodal, *S*-dG phosphoramidite **16** and the CPG-loaded *S*-dG solid support (**18**), we started with the known 3′,5′-bis-*O*-benzyl protected compound **12** (Scheme 2) (65). As before, formation of the *N*-isobutyryl amide **13** and removal of all benzyl groups by catalytic hydrogenation provided the key intermediate **14**, which was converted in a similar manner as before to the desired phosphoramidite building block (**16**) and the 3′-*O*-succinyl derivative **17**, which was loaded onto the CPG resin to give **18**.

In both cases, the phosphitylation reaction was slower than the comparable reaction with natural nucleosides and the yields were moderate. The resulting phosphoramidites **9** and **16** were stable and could be purified on silica gel and stored for a long time without the loss of reactivity.

Oligonucleotide synthesis

Oligonucleotide synthesis was performed using controlled pore glass (CPG) supports. The addition of the locked, methanocarba nucleoside phosphoramidites was performed manually using 10–15 mg of the appropriate monomers with an extended coupling time of 10 min. The rest of the sequences were assembled using an automated DNA synthesizer. After addition of the *N*-methanocarba-dG phosphoramidite, oxidation of phosphites was performed with a *t*-butylhydroperoxide (tBuOOOH) solution as described elsewhere (31) to avoid iodine degradation of the phosphodiester backbone at the pseudosugar position. Using these optimized synthesis conditions, all modified oligonucleotides were successfully synthesized and characterized by HPLC analysis of enzyme digestions and mass spectrometry. The isolated yields after HPLC purification and desalting were in the range of those obtained for unmodified oligonucleotides.

Thermal stability by CD and UV spectroscopy

In order to define the effects of the modifications imposed by the rigid pseudosugar rings, melting curves of the modified samples were performed by CD and UV spectroscopy and compared with the unmodified sequence. The appearance of the CD spectra was consistent with an antiparallel G-quartet architecture characterized by a positive band at 248 nm, a positive maximum at 295 nm and a negative maximum at 265 nm (Figure 5). The CD spectrum of a parallel quadruplex in contrast presents a positive maximum near 265 nm. A reversal in topology from antiparallel to parallel folding can be induced by the selective substitution of 2′-deoxyguanosine for riboguanosine (20), which can be followed by changes in the CD spectra.

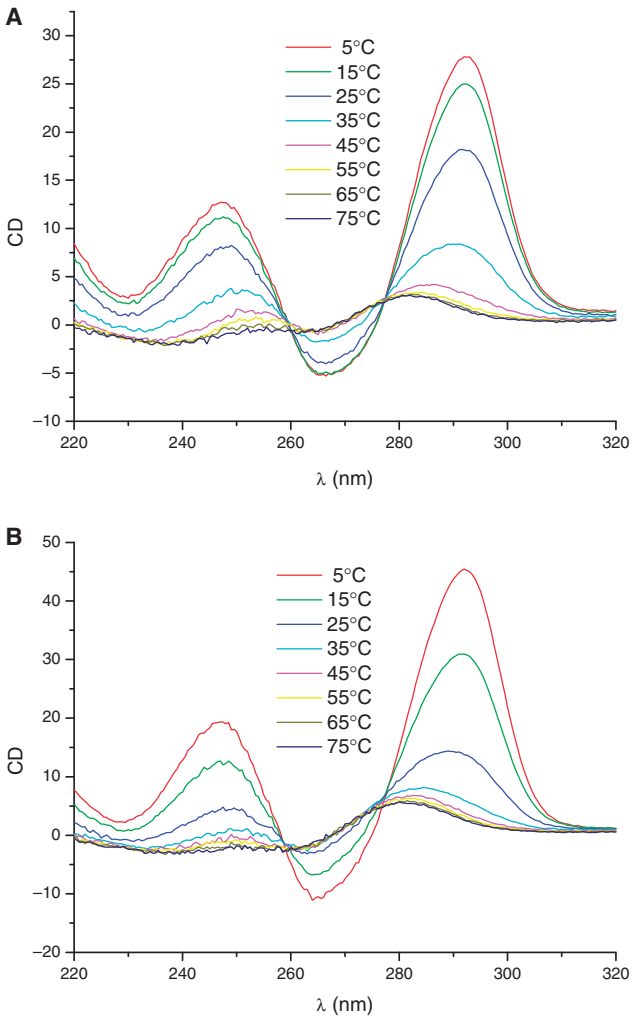

Figure 5. (**A**) CD spectra of TBA-d15G*N* at different temperatures. (**B**) CD spectra of TBA-d15G*S* at different temperatures.

In our experiments, CD spectra of native and modified TBA derivatives presented a maximum at 295 nm at all temperatures indicating an antiparallel quadruplex structure for all the TBA derivatives studied in this work. The melting temperatures for the TBA-dG5*S*, TBA-dG10*S*, TBA-dG14*S*, TBA-dG15*N* and TBA-dG15*S* were 44.7°C, 40.7°C, 45°C, 28.4°C and 17°C, respectively (Table 2), indicating a lower thermal stability of the two quadruplexes modified at position 15, but a similar stability as native TBA (T_m 46°C) for the quadruplexes carrying the same sugar pucker and *syn* glycoyl bond orientation present in the unmodified TBA (TBA-dG5*S*, TBA-dG10*S*, TBA-dG14*S*). TBA-dG14*N* instead gave a monotonous decrease of the CD signal at 295 nm without apparent T_m. A similar result was obtained when the melting curves were followed by UV (295 nm) at a concentration of 6 μM (UV experiment, Table 2) instead of 80 μM (CD experiment).

The combined results from the CD and UV studies (Table 2) indicate that relative to the T_m of the unmodified TBA (45–46°C), only TBA-dG5*S*, TBA-dG10*S* and TBA-dG14*S*, in which the modified methanocarba derivative

Table 2. Melting temperatures of thrombin binding aptamers carrying methanocarba-dG nucleosides

Sequence	T_m (°C), CD (80 μM)[a]	T_m (°C), UV (6 μM)[b]
TBA	46.0	48.6
TBA-dG15*N*	28.4	35.0
TBA-dG15*S*	17.0	22.1
TBA-dG14*S*	45.0	47.3
TBA-dG14*N*	n.d.[c]	n.d.[c]
TBA-dG5*S*	44.7	47.3
TBA-dG10*S*	40.7	42.2

[a]5 mM KCl, 10 mM potassium phosphate buffer pH 6.9.
[b]100 mM KCl, 10 mM sodium cacodylate buffer pH 6.9.
[c]Not determined because curves were not cooperative and only a fraction of the transition (if any) were observed.

mimics the native's *S* sugar pucker and the *syn* conformation of the guanine ring, generate G-quartets of similar stability to the unmodified TBA. The totally opposite arrangement represented by TBA-dG14*N*, where the TBA's conformational preferences at position 14 are completely reversed, was very destabilizing. The other combinations, representing a mismatch of either pseudosugar pucker or glycosyl torsion angle, relatively to the native TBA, induced different degrees of destabilization. The data support the claim that a reversal in the glycosyl torsion angle appears to be more critical for the stability of the G-quartet than a mismatch of the sugar pucker, since the drop in thermal stability was about 10°C more severe for TBA-dG15*S* than for TBA-dG15*N*. The structural impact that the introduction of both types of distortions has on the global architecture of the corresponding tetraplexes is discussed below in detail as ascertained by NMR experiments and MD simulations.

^{1}H NMR studies

The imino proton region of the NMR spectra of the modified aptamers clearly indicates the formation of quadruplex structures. In the case of TBA-dG15*N*, TBA-dG14*S*, TBA-dG5*S* and TBA-dG10*S*, a single set of sharp and well-dispersed imino signals are observed between 10.0 and 12.5 ppm (Figure 6). These spectra are consistent with a single G-quadruplex structure similar to that of the unmodified aptamer (9). In contrast, the exceeding number of imino signals in the NMR spectra of TBA-dG15*S* at 5°C suggests the presence of several species in equilibrium. The broad band observed around 11.0 ppm may arise from a higher molecular weight species or from conformational heterogeneity due to multiple low populated conformers. Nevertheless, the set of sharp and more intense imino signals in the 1D spectra and the NOESY cross-peaks of this modified aptamer (data not shown) present features that closely resemble the spectra of the unmodified TBA, indicating that the major conformer of TBA-dG15*S* adopts a structure similar to the one of the unmodified TBA. The NMR spectra of TBA-dG14*N* at 5°C shown in Figure 6 also present a mixed of sharp signals and a large broad band around 11.0 ppm, but in this cases the sharp signals have a much lower intensity, indicating that this aptamer adopt multiple structures with no major prevailing conformer.

Unfolding transitions were followed by NMR. The melting behaviour of the four modified aptamers is consistent with the thermal stability data obtained by UV and CD spectroscopies. In the case of TBA-dG15*N*, TBA-dG14*S*, TBA-dG5*S* and TBA-dG10*S*, exchangeable protons are observed at temperatures above the denaturation midpoint, suggesting very slow dissociation kinetics (Figure 6). This effect is also observed in unmodified TBA, but it is more pronounced in the modified TBAs with locked nucleotides in stabilizing positions. This suggests that the presence of a locked nucleotide slows down the denaturation kinetics of the whole quadruplex. Interestingly, the broad signals around 11.0 ppm in TBA-dG15*S* can also be observed at temperatures quite above its T_m. A broad band is also observed in the case of TBA-dG15*N* at 45°C. It is tempting to assign these broad signals to the denaturation intermediate hypothesized by Mao and Gmeiner using hydrogen exchange experiments on unmodified TBA in the presence of Sr^{2+} cations (12). A deceleration of the denaturation kinetics might be a general phenomena of this kind of antiparallel quadruplex containing locked nucleotides, allowing in some cases the observation of NMR signals from denaturation intermediates. The fact that a single modification at the 3′ terminus of the TBA can affect its folding/unfolding process may have an influence in its binding to thrombin (18).

The structures of TBA-dG15*N* and TBA-dG14*S* were studied in more detail by bidimensional NMR spectroscopy. The close similarity in their structures and the unmodified TBA is apparent in the NOESY spectra (Figure 7). Assignment of most of the exchangeable and non-exchangeable protons in these two aptamers was carried out on the basis of previously reported assignments of TBA (9) (see Supplementary Data for assignment tables). The pattern of NOEs observed indicated that the global backbone conformation is very similar. The strong intensities of intraresidue NOE cross peaks between the H8 protons of G and H1′ protons confirmed the *syn* conformation for the glycosyl angle of dG1, dG5, dG10 and dG14. The NOESY spectra of TBA and TBA-dG14*S* are nearly identical with minimal changes in the chemical shifts of residues around the modification. However, more pronounced changes are observed in TBA-dG15*N*, like some different NOEs between dG15 and T9 relative to the unmodified aptamer. This could be explained by the rigid conformation of the pseudo sugar that produces a slight local deformation in the G-quartet structure with a different orientation of the T9.

Assignment of the bicyclo[3.1.0]hexane pseudosugars could be also performed for TBA-dG15*N* and TBA-dG14*S*. Overlaid NOESY spectra of these two samples and the unmodified TBA are shown in Figure 7. Bicyclo-hexane spin systems were identified in the TOCSY spectra in D_2O. The two additional resonances (H7′/H7″ according to the naming scheme shown in Figure 7) and the high field shift of these protons (~1.0–1.5 ppm) allowed for distinguishing the bicyclo-hexane from the deoxyriboses spins systems. Starting from H7′/H7″ resonances, the remaining bicyclo-hexane

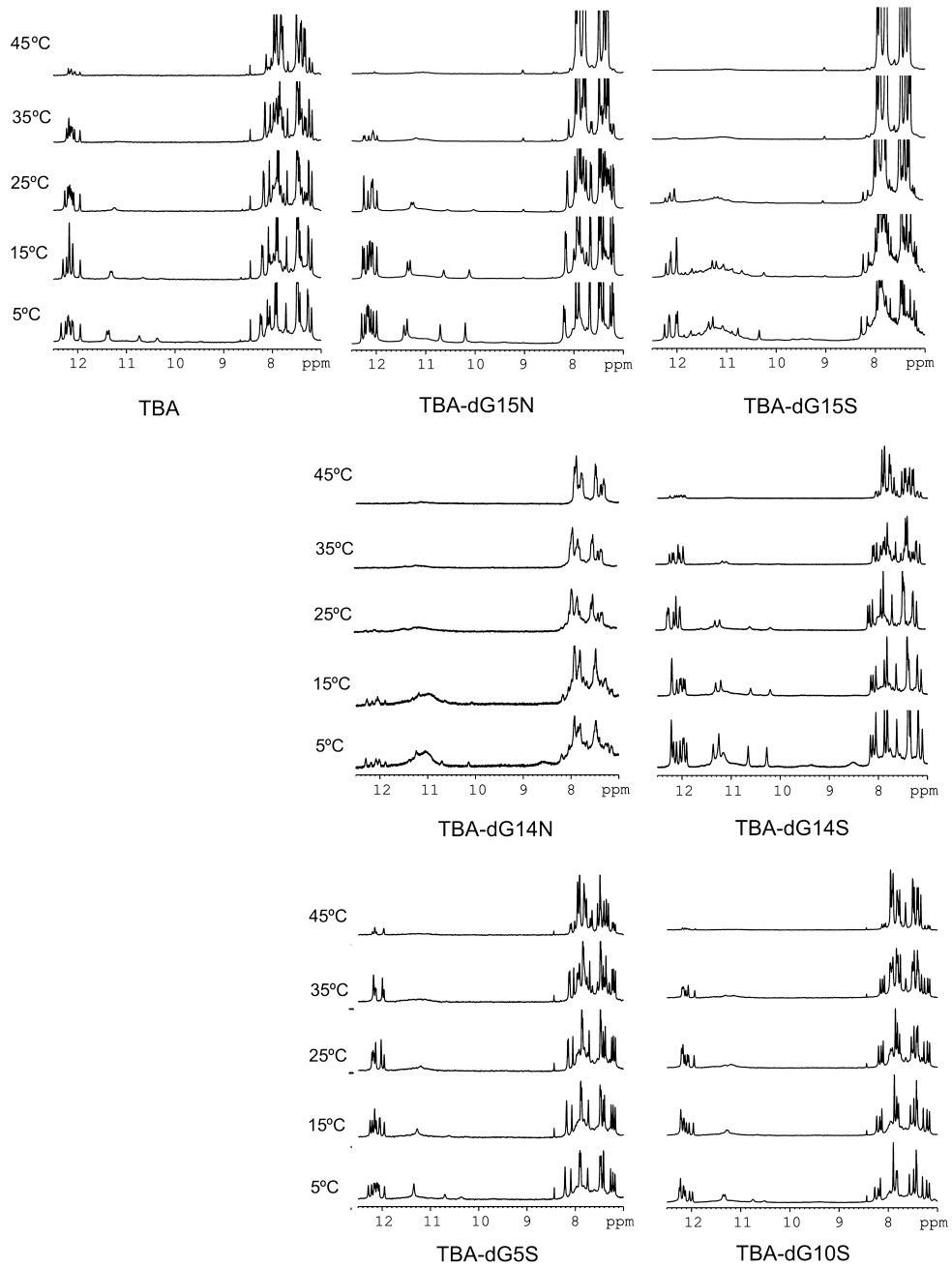

Figure 6. Imino regions of the NMR spectra of the different TBA aptamers in H_2O at different temperatures.

protons were assigned by combining through-bond TOCSY connections with through-distances cross-peaks derived from NOESY experiments recorded at a short mixing time. The glycosyl angle of the locked nucleotides can be determined from the intraresidual H8-sugar NOE intensities. Thus, the very strong NOEs between H7′/7″ and H8 of G14S in TBA-dG14, as well as the medium or weak intensity of the H6′–H8 NOE (see green spectra in Figure 7), clearly indicates the glycosidic conformation is *syn*. On the other hand, the strong H6′–H8 and H3′–H8 NOEs and the medium or weak H1′–H8 cross-peak (yellow spectra in Figure 7) show that the glycosidic conformation of G15N in TBA-dG15*N* is *anti*. This analysis could not be carried out in the case of TBA-dG15*S* and TBA-dG14*N*, since the presence of multiple species impedes the complete assignment of the NMR spectra.

Molecular dynamics analysis of natural and modified aptamers

As found in previous MD simulations, which extended to the microsecond range (57), the unmodified TBA behaved like a very stable structure during the 10×10 ns simulations (0.1 μs effective simulation time), sampling conformational regions very close to those expected from the NMR structures (Figure 8). One or two ions remained

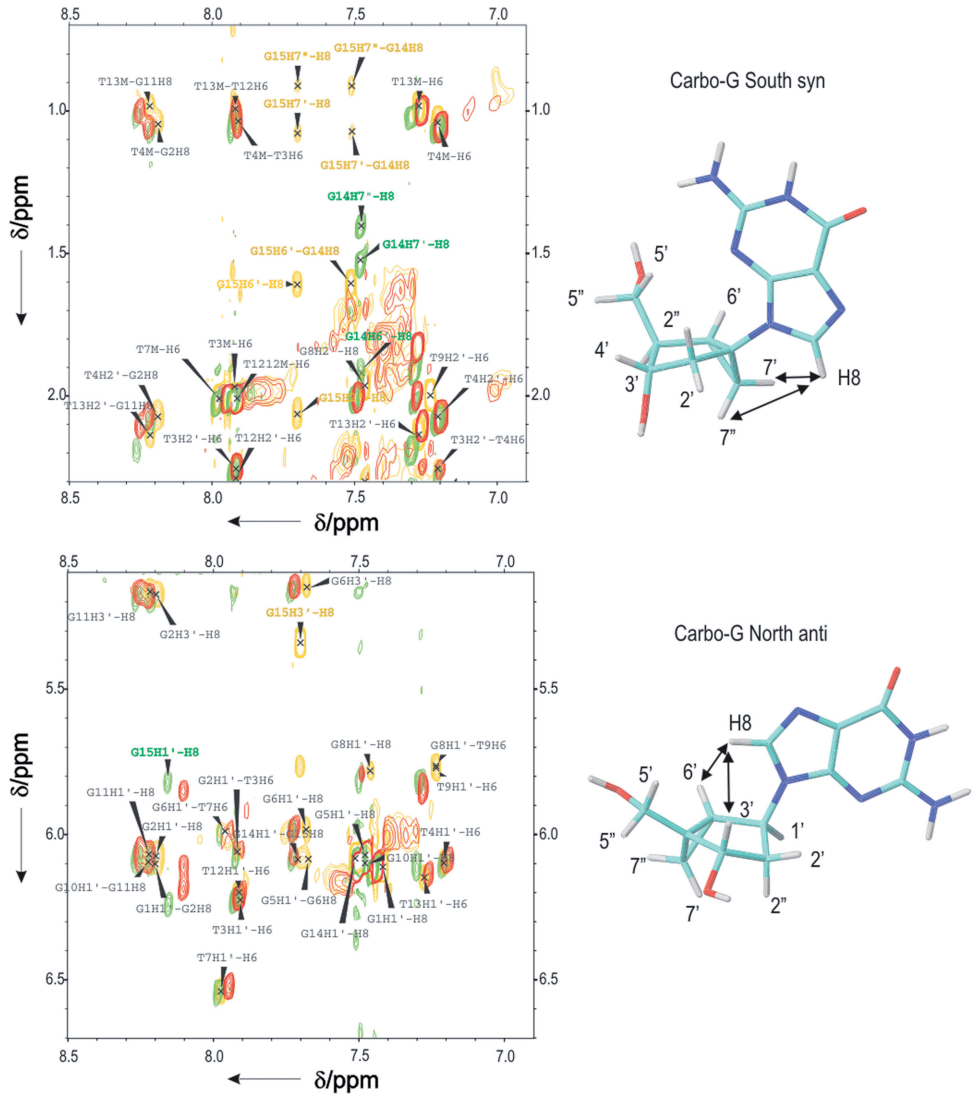

Figure 7. Selected regions of NOESY spectra of unmodified TBA (red), TBA-dG15*N* (yellow) and TBA-dG15*S* (green). Locked-nucleotide resonances are labelled in their respective colour, according to the numbering scheme shown. The conformation of the glycosyl angle can be determined from some key strong NOEs, indicated with arrows.

inside the central channel during all the trajectories and the G–G pattern of hydrogen-bond interactions was maintained without distortions for the entire set of simulations. The TBA-dG14*S* trajectories are in practice identical to those of the unmodified TBA, confirming that the introduction of the *S*-methanocarba-2′-dG at a position where 2′-dG is found in the *S-syn* conformation does not have any negative structural impact. The 10 trajectories of TBA-dG15*N* and the 10 trajectories of TBA-dG15*S* also sampled conformations not far from those of the unmodified aptamer, in good agreement with NMR measures. Small distortions were observed (data not shown) in the χ angle of the bonding partners dG1 and dG10 and the stacking partner dG14, and in the puckering of dG15. In the case of TBA-dG15*N*, there were small changes in the χ angle around the neighbours of dG15 (dG1, dG10 and dG14) and the puckering of dG14. It is possible that longer simulations (micro to millisecond long) could lead to the disruption of some of these aptamers (for example TBA-dG15*S* which shows a T_m below our working temperature), but in general all structures appeared to be reasonably stable, confirming the unmistakable plasticity of the G-DNA.

Trajectories for the TBA-dG14*N* aptamer showed a quite different scenario, since ultra-fast unfolding (<10 ns) was observed in 3 of the 10 trajectories, illustrating the large instability of the structure (Figure 8) already predicted from experimental measurements. The unfolded trajectories led to the corruption of the G-quadruplex structure with separation of the terminal guanines, which originally form half of the guanine quartet, in agreement with the mechanism already suggested by NMR experiments (*vide supra*). During our MD simulations, the unfolded conformation retained the antiparallel hairpin-like structure due to the still existing hydrogen bond interaction between non-terminal guanines and the

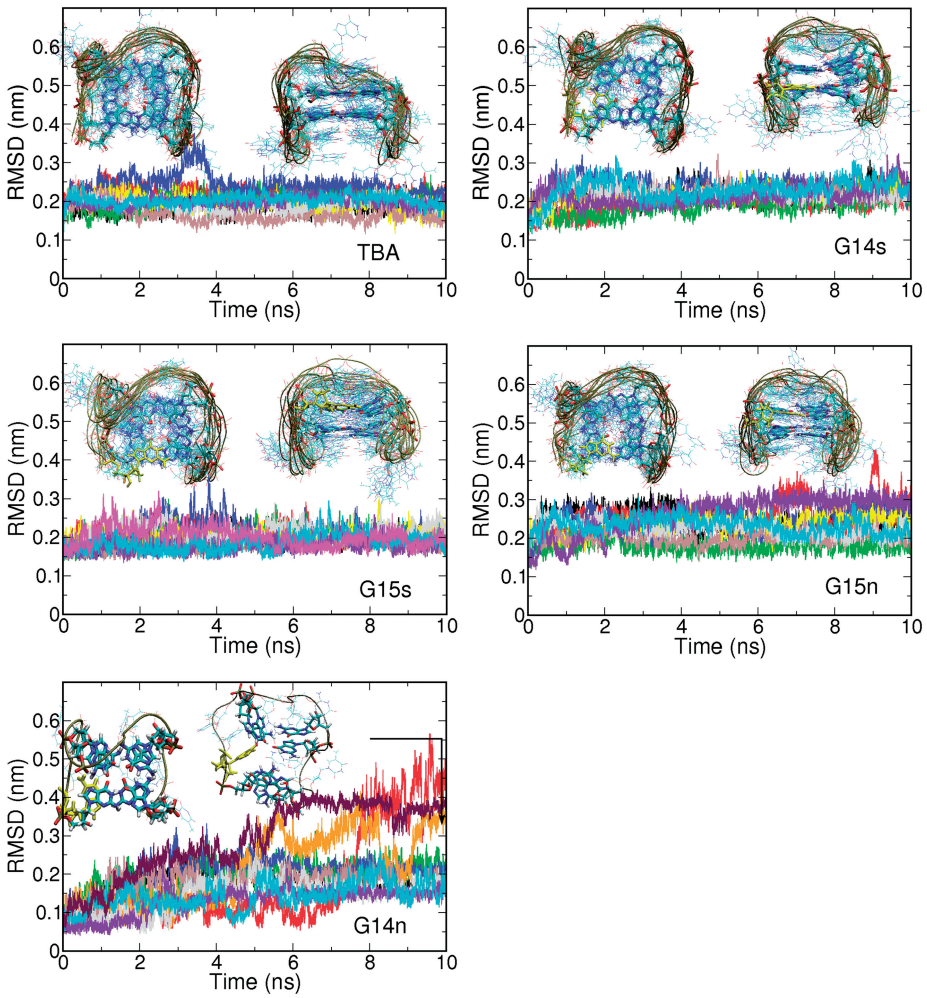

Figure 8. Evolution of the RMSD (from NMR structure) in MD simulations performed for different variants of the thrombin-binding aptamer (TBA) containing only 2′-deoxyguanosine or methanocarba-dG nucleotides at selected positions. In cases where the structure is not corrupted, the frontal and top view of the system as observed in the 10 ns simulations is displayed. For the TBA-dG14*N* system an example of the structure obtained after unfolding is displayed.

stabilizing stacking interactions, but the similarity to the original tetrad is completely lost and the structure sampled a much wider configurational space, thus behaving similar to a random coil. Clearly, the MD simulations strongly support the NMR, CD and UV derived models, providing an atomistic view of the structural impact of biasing conformational preferences on the scaffold of the TBA aptamer.

CONCLUSIONS

Conformationally locked *N* and *S* 2′-deoxyguanosine nucleosides built on a bicyclo[3.1.0]hexane template (methanocarba nucleosides) were incorporated into TBA aptamers at four specific positions where the 2′-deoxyguanosines display different conformational preferences. Contrary to the situation in B-DNA, where the methanocarba substitutions had a small effect on the global stability of the duplex (32–34), the stability of the TBA aptamer was very dependent on the type and location of the methanocarba-dG nucleotides. The substitution of the native *S*(*syn*)dG in TBA with an equivalent, locked *S*(*syn*)dG at positions 5, 10 and 14 maintained stability except for a slight decrease on T_m at position 10. Positions 5 and 10 are located in the same bottom G-quartet, but position 10 is located in the upper G-quartet. This result indicates that both quartets are not equivalent and our *S*(*syn*)dG analogue accommodates better on the lower quartet.

The destabilization observed when the native *S*(*anti*)dG at position 15 was replaced with a *S*(*syn*)dG was greater than when it was replaced by a *N*(*anti*)dG, supporting the concept that the glycosyl conformation is more restrictive for TBA stability than the sugar puckering. Finally, the substitution of *S*(*syn*)dG at position 14 by a locked *N*(*anti*)dG led to a dramatic destabilization of the TBA, which according to NMR and MD simulations begins with the structural disruption of the terminal G–G pairs, followed quite closely by the formation of other global conformations that were previously assigned to denaturation intermediates but never observed in the unmodified TBA.

Taken together our theoretical and experimental results establish that both *N*- or *S*-methanocarba nucleosides represent uniquely discriminating probes to study the role of *North*/*South* puckering and *syn*/*anti* conformations on the stability of the antiparallel TBA quadruplex and possibly other aptamers with a similar architecture. These locked analogues also have an impact in the quadruplex formation/denaturation kinetics and helped us visualize a denaturation intermediate whose existence had only been hypothesized.

SUPPLEMENTARY DATA

Supplementary Data are available at NAR Online.

FUNDING

Spanish Ministry of Education [BFU2007-63287, NAN2004-09415-C05-5, BIO2006-01602, CTQ2007-68014-C02-02, Consolider Escience Project]; the Generalitat de Catalunya [2005/SGR/00693, 2006PIV00028]; the Instituto de Salud Carlos III [CIBER-BBN, CB06/01/0019]; the National Institute of Bioinformatics, the Marcelino Botin foundation, the COST project (G4-net, MP0802), and the Intramural Research Program of the National Institutes of Health, National Cancer Institute, Center for Cancer Research. Funding for open access charge: FUNMOL, FP7-NMP-213382-2.

Conflict of interest statement. None declared.

REFERENCES

1. Ellington,A.D. and Szostak,J.W. (1990) *In vitro* selection of RNA molecules that bind specific ligands. *Nature*, **346**, 818–822.
2. Tuerk,C. and Gold,L. (1990) Systematic evolution of ligands by exponential enrichment: RNA ligands to bacteriophage T4 DNA polymerase. *Science*, **249**, 505–510.
3. Brody,E.N. and Gold,L. (2000) Aptamers as therapeutic and diagnostic agents. *Rev. Mol. Biotech.*, **74**, 5–13.
4. Kusser,W. (2000) Chemically modified nucleic acid for *in vitro* selections: evolving evolution. *Rev. Mol. Biotech.*, **74**, 27–38.
5. Bock,L.C., Griffin,L.C., Latham,J.A., Vermaas,E.H. and Toole,J.J. (1992) Selection of single-stranded DNA molecules that bind and inhibit human thrombin. *Nature*, **355**, 564–566.
6. Griffin,L.C., Tidmarsh,G.F., Bock,L.C., Toole,J.J. and Leung,L.L. (1993) *In vivo* anticoagulant properties of a novel nucleoside-based thrombin inhibitor and demonstration of regional anticoagulation in extracorporeal circuits. *Blood*, **81**, 3271–3276.
7. Wang,K.Y., McCurdy, Shea,R.G., Swaminathan,S. and Bolton,P.H. (1993) A DNA aptamer which binds to and inhibits thrombin exhibits a new structural motif for DNA. *Biochemistry*, **32**, 1899–1904.
8. Macaya,R.F., Schultze,P., Smith,F.W., Roe,J.A. and Feigon,J. (1993) Thrombin-binding DNA aptamer forms a unimolecular quadruplex structure in solution. *Proc. Natl Acad. Sci. USA*, **90**, 3745–3749.
9. Schultze,P., Macaya,R.F. and Feigon,J. (1994) Three-dimensional solution structure of the thrombin-binding DNA aptamer d(GGTTGGTGTGGTTGG). *J. Mol. Biol.*, **235**, 1532–1547.
10. Padmanabhan,K., Padmanabhan,K.P., Ferrara,J.D., Sadler,J.E. and Tulinsky,A. (1993) The structure of alfa-thrombin inhibited by a 15-mer single-stranded DNA aptamer. *J. Biol. Chem.*, **268**, 17651–17654.
11. Kelly,J.A., Feigon,J. and Yeates,T.O. (1996) Reconciliation of the X-ray and NMR structures of the thrombin-binding aptamer d(GGTTGGTGTGGTTGG). *J. Mol. Biol.*, **256**, 417–422.
12. Mao,X. and Gmeiner,W.H. (2005) NMR study of the folding-unfolding mechanism for the thrombin-binding DNA aptamer d(GGTTGGTGTGGTTGG). *Biophys. J.*, **113**, 155–160.
13. Fialova,M., Kypr,J. and Vorlickova,M. (2006) The thrombin binding aptamer GGTTGGTGTGGTTGG forms a bimolecular guanine tetraplex. *Biochem. Biophys. Res. Comm.*, **344**, 50–54.
14. Marathias,V.M., Sawicki,M.J. and Bolton,P.H. (1999) 6-Thioguanine alters the structure and stability of duplex DNA and inhibits quadruplex DNA formation. *Nucleic Acids Res.*, **27**, 2860–2867.
15. Lopez de la Osa,J., Gonzalez,C., Gargallo,R., Rueda,M., Cubero,E., Orozco,M., Aviñó,A. and Eritja,R. (2006) Destabilization of quaduplex DNA by 8-aminoguanine. *Chem. BioChem.*, **7**, 46–48.
16. Martino,L., Virno,A., Randazzo,A., Virgilio,A., Esposito,V., Giancola,C., Bucci,M., Cirino,G. and Mayol,L. (2006) A new modified thrombin binding aptamer containing a 5'-5' inversion of polarity site. *Nucleic Acids Res.*, **34**, 6653–6662.
17. Pagano,B., Martino,L., Randazzo,A. and Giancola,C. (2007) Stability and binding properties of a modified thrombin binding aptamer. *Biophys. J.*, **94**, 562–569.
18. Virno,A., Randazzo,A., Giancola,C., Bucci,M., Cirino,G. and Mayol,L. (2007) A novel thrombin aptamer containing a G-LNA residue. *Biorg. Med. Chem.*, **15**, 5710–5718.
19. Bonifacio,L., Church,F.C. and Jarstfer,M.B. (2008) Effect of locked-nucleic acid on a biologically active G-quadruplex. A structure-activity relationship of the thrombin aptamer. *Int. J. Mol. Sci.*, **9**, 422–433.
20. Peng,C.G. and Damha,M.J. (2007) G-quadruplex induced stabilization by 2′-deoxy-2′-fluoro-D-arabinonucleic acids (2′F-ANA). *Nucleic Acids Res.*, **35**, 4977–4988.
21. Tang,C.F. and Shafer,R.H. (2006) Engineering the quadruplex fold: nucleoside conformation determines both folding topology and molecularity in guanine quadruplexes. *J. Am. Chem. Soc.*, **128**, 5966–5973.
22. Rodriguez,J.B., Marquez,V.E., Nicklaus,M.C., Mitsuya,H. and Barchi,J.J. (1994) Conformationally locked nucleosides analogues. Synthesis of dideoxycarbocyclic nucleosides analogues structurally related to neplanocin C. *J. Med. Chem.*, **37**, 3389–3399.
23. Obika,S. (2004) Development of bridged nucleic acids analogues for antigene technology. *Chem. Pharm. Bull.*, **52**, 1399–1404.
24. Koshkin,A.A., Rajwanski,V.K. and Wengel,J. (1998) Novel convenient syntheses of LNA[2.2.1]bicyclo nucleosides. *Tetrahedron Lett.*, **39**, 4381–4384.
25. Renneberg,D., Boiliong,E., Reber,U., Schumperli,D. and Leumann,C.J. (2002) Antisense properties of tricycle-DNA. *Nucleic Acids Res.*, **30**, 2751–2757.
26. Opalinska,J.B., Kalota,A., Gifford,L.K., Lu,P.Z., Jen,K.Y., Pradeepkumar,P.I., Barman,J., Kim,T.K., Swider,C.R., Chatopadhyaya,J. *et al.* (2004) Oxitane modified conformationally constrained, antisense oligodeoxyribonucleotides function efficiently as gene silencing molecules. *Nucleic Acids Res.*, **32**, 5791–5799.
27. Jepsen,J.S., Sorensen,M.D. and Wengel,J. (2004) Locked nucleic acids: A potent nucleic acid analog in therapeutics and biotechnology. *Oligonucleotides*, **14**, 130–146.
28. Rodriguez,J.B., Marquez,V.E., Nicklaus,M.C. and Barchi,J.J. (1993) Synthesis of cyclopropane-fused dideoxycarbocyclic nucleosides structurally related to neoplanocin C. *Tetrahedron Lett.*, **34**, 6233–6236.
29. Marquez,V.E., Siddiqui,M.A., Ezzitouni,A., Puss,P., Wang,J.Y., Wagner,R.W. and Matteucci,M.D. (1996) Nucleosides with a twist. Can fixed forms of sugar ring pucker influence biological activity in nucleosides and oligonucleotides. *J. Med. Chem.*, **39**, 3739–3747.
30. Wang,P., Nicklaus,M.C., Marquez,V.E., Brank,A.S., Christman,J.K., Banavali,N.K. and MacKerrell,A.D. Jr. (2000) Use of oligodeoxyribonucleotides with conformationally constrained abasic sugar targets to probe the mechanism of base flipping by *Hha*I DNA (Cytosine C5)-mehtyltransferase. *J. Am. Chem. Soc.*, **122**, 12422–12434.
31. Maier,M.A., Choi,Y., Gaus,H., Barchi,J.J., Marquez,V.E. and Manoharan,M. (2004) Synthesis and characterization of

oligonucleotides containing conformationally constrained bicyclo[3.1.0]hexane pseudosugar analogs. *Nucleic Acids Res.*, **32**, 3642–3650.
32. Wu,Z., Madeira,M., Barchi,J.J., Marquez,V.E. and Bax,A. (2005) Changes in DNA bending induced by restricting nucleotide ring pucker studied by weak alignment NMR spectroscopy. *Proc. Natl Acad. Sci. USA*, **102**, 24–28.
33. Madeira,M., Wu,J., Bax,A., Shenoy,S., O'Keefe,B., Marquez,V.E. and Barchi,J.J. (2005) Engineering DNA topology with locked nucleosides: A structural study. *Nucleosides Nucleotides, Nucleic Acids*, **24**, 687–690.
34. Madeira,M., Shenoy,S., Van,Q.N., Marquez,V.E. and Barchi,J.J. (2007) Biophysical studies of DNA modified with conformationally constrained nucleotides: comparison of 2′-exo (north) and 3′-exo (south) 'locked' templates. *Nucleic Acids Res.*, **35**, 1978–1991.
35. Saenger,W. (1984) *Principles of Nucleic Acid Structure*. Springer, New York, NY.
36. Marquez,V.E., Ben-Kasus,T., Barchi,J.J. Jr, Green,K.M., Nicklaus,M.C. and Agbaria,R. (2004) Experimental and structural evidence that herpes 1 kinase and cellular DNA polymerase(s) discriminate on the basis of sugar pucker. *J. Am. Chem. Soc.*, **126**, 543–549.
37. Kumar,A., Ernst,R.R. and Wutrich,K. (1980) A two-dimensional nuclear Overhauser enhancement (2D NOE) experiment for the elucidation of complete proton-proton cross-relaxation networks in biological macromolecules. *Biochem. Biophys. Res. Comm.*, **95**, 1–6.
38. Braunschweiler,L. and Ernst,R.R. (1983) Coherence transfer by isotropic mixing: application to proton correlation spectroscopy. *J. Magn. Reson.*, **53**, 521–528.
39. Redfield,A.G. and Kunz,S.D. (1975) Quadrature Fourier NMR detection-simple multiplex for dual detection and discussion. *J. Magn. Reson.*, **19**, 250–254.
40. Goddard,T.D. and Kneller,D.G. (2004) *SPARKY 3*, University of California, San Francisco, USA.
41. Mastryukov,V.S., Osina,E.L., Vilkov,L.V. and Hildebrandt,R.L. (1977) The zero-point-average structure of bicyclo[3.1.0]hexane as determined by electron diffraction and microwave spectroscopy. *J. Am. Chem. Soc.*, **99**, 6855–6861.
42. Marquez,V.E., Ezzitouni,A., Russ,P., Siddiqui,M.A., Ford,H., Feldman,R.J., Mitsuya,H., George,C. and Barchi,J.J. Jr. (1998) HIV-1 reverse transcriptase can discriminate between two conformationally locked carbocyclic AZT triphosphate analogues. *J. Am. Chem. Soc.*, **120**, 2780–2789.
43. Marquez,V.E., Russ,P., Alonso,R., Siddiqui,M.A., Hernández,S., George,C., Nicklaus,M., Dai,F. and Ford,H. (1999) Synthesis of conformationally restricted carbocyclic nucleosides. The role of the O4′-oxigen in the key hydration step of adenosine deaminase. *Helv. Chim. Acta*, **82**, 2119–2129.
44. Mjöberg,P.J. and Almlöf,J.A. (1978) Conformational study of bicyclo[3.l.0]hexane and the 3-bicyclo[3.l.0]hexane carbonium ion: an ab initio SCF investigation. *Chem. Phys.*, **29**, 201–208.
45. Skancke,P.N. (1982) The molecular and electronic structure of bicyclo[l.l.0]butane, bicyclo[2.1.0]pentane, and bicyclo[3.1.0]hexane as obtained by ab initio SCF Calculations. *J. Mol. Struct.*, **86**, 255–266.
46. Siam,K., Ewbank,J.D., Schafer,L. and Van Alsenoy,C. (1987) A critical comparison of the *ab initio* geometry and zero-point-average structure of bicyclo[3.l.0lhexane. *J. Mol. Struct.*, **150**, 121–128.
47. Okazaki,R., Niwa,J. and Kato,S. (1988) An ab initio molecular orbital study of the conformations of bicyclo[3.l.0]hexane derivatives. *Bull. Chem. Soc. Jpn.*, **61**, 1619–1624.
48. Frisch,M.J., Trucks,G.W., Schlegel,H.B., Scuseria,G.E., Robb,M.A., Cheeseman,J.R., Montgomery,J.A., Vreven,T., Kudin,K.N., Burant,J.C. *et al.* (2004) *Gaussian 03*, Revision D.02, Gaussian, Inc., Wallingford, CT.
49. Orozco,M., Bachs,M. and Luque,F.J. (1995) Development of optimized MST/SCRF methods for semiempirical calculations: the MNDO and PM3 Hamiltonians. *J. Comput. Chem.*, **16**, 563–575.
50. Luque,F.J., Zhang,Y., Aleman,C., Bachs,M., Gao,J. and Orozco,M. (1996) Solvent effects in chloroform solution: parametrization of the MST/SCRF continuum model. *J. Phys. Chem.*, **100**, 4269–4276.
51. Luque,F.J., Aleman,C., Bachs,M. and Orozco,M. (1996) Extension of the MST/SCRF method to organic solvents: ab initio and semiempirical parametrization for neutral solutes in CC14. *J. Comput. Chem.*, **17**, 806–820.
52. Curutchet,C., Orozco,M. and Luque,F.J. (2001) Solvation in octanol: parametrization of the continuum MST model. *J. Comput. Chem.*, **22**, 1180–1193.
53. Miertus,S. and Tomasi,J. (1982) Approximate evaluations of the electrostatic free energy and internal energy changes in solution processes. *Chem. Phys.*, **65**, 239–245.
54. Miertus,S., Scrocco,E. and Tomasi,J. (1981) Electrostatic interactions of a solute with a continuum. A direct utilization of *ab initio* molecular potentials for the prevision of solvent effects. *Chem. Phys.*, **55**, 117–129.
55. Cheatman,T.E. III, Cieplack,P. and Kollman,P.A. (1999) A modified version of the Cornell et al. force field with improved sugar pucker phases and helical repeat. *J. Biomol. Struct. Dyn.*, **16**, 845–862.
56. Bayly,C.I., Cieplack,P., Cornell,W. and Kollman,P.A. (1993) A well-behaved electrostatic potential based method using charge restraints for determining atom-centered charges: The RESP model. *J. Phys. Chem.*, **97**, 10269–10280.
57. Perez,A., Marchan,I., Svozil,D., Sponer,J., Cheatham,T.E. III, Laugthon,C.A. and Orozco,M. (2007) Refinement of the AMBER force field for nucleic acids: improving the description of alpha/gamma conformers. *Biophys. J.*, **92**, 3817–3829.
58. Jorgensen,W.L., Chandrasekhar,J., Madura,J.D., Impey,R.W. and Klein,M.L. (1983) Comparison of simple potential functions for simulating liquid water. *J. Chem. Phys.*, **79**, 926–935.
59. Hess,B., Kutzer,C., van der Spoel,D. and Lindahl,E. (2008) GROMACS 4: algorithms for highly efficient, load-balanced, and scalable molecular simulation. *J. Chem. Theory Comput.*, **4**, 435–447.
60. Dardem,T., York,D. and Pedersen,L (1983) Particle mesh Ewald: an $N.\log(N)$ method for Ewald sums in large systems. *J. Chem. Phys.*, **98**, 10089–10092.
61. Miyamoto,S. and Kollman,P.A. (1992) SETTLE: an analytical version of the SHAKE and RATTLE algorithm for rigid water models. *J. Comput. Chem.*, **13**, 952–962.
62. Hess,B. (2008) P-LINCS: a parallel linear constraint solver for molecular simulation. *J. Chem. Theory Comput.*, **4**, 116–122.
63. Bussi,G., Donadio,D. and Parrinello,M. (2007) Canonical sampling through velocity rescaling. *J. Chem. Phys.*, **126**, 014101/1–014101/7.
64. Berendsen,H.J.C., Postma,J.P.M., van Gunsteren,W.F., Dinola,A. and Hook,J.R. (1984) Molecular-dynamics with coupling to an external bath. *J. Chem. Phys.*, **81**, 3684–3690.
65. Ezzitouni,A., Barchi,J.J. Jr. and Marquez,V.E. (1997) Conformationally locked carbocyclic nucleosides built on a bicyclo[3.1.0]hexane template with a fixed southern conformation. Synthesis and antiviral activity. *J. Chem. Soc. Perkin Trans.* **I**, 1073–1078.